

# Author's Accepted Manuscript

Inter-subject variability Effects on the primary stability of a short cementless femoral stem

Mamadou T. Bah, Junfen Shi, Markus O. Heller, Yanneck Suchier, Fabien Lefebvre, Philippe Young, Leonard King, Doug G. Dunlop, Mick Boettcher, Edward Draper, Martin Browne



PII: S0021-9290(15)00053-6  
DOI: <http://dx.doi.org/10.1016/j.jbiomech.2015.01.037>  
Reference: BM7002

To appear in: *Journal of Biomechanics*

Accepted date: 26 January 2015

Cite this article as: Mamadou T. Bah, Junfen Shi, Markus O. Heller, Yanneck Suchier, Fabien Lefebvre, Philippe Young, Leonard King, Doug G. Dunlop, Mick Boettcher, Edward Draper, Martin Browne, Inter-subject variability Effects on the primary stability of a short cementless femoral stem, *Journal of Biomechanics*, <http://dx.doi.org/10.1016/j.jbiomech.2015.01.037>

This is a PDF file of an unedited manuscript that has been accepted for publication. As a service to our customers we are providing this early version of the manuscript. The manuscript will undergo copyediting, typesetting, and review of the resulting galley proof before it is published in its final citable form. Please note that during the production process errors may be discovered which could affect the content, and all legal disclaimers that apply to the journal pertain.

# Inter-Subject Variability Effects on the Primary Stability of a Short Cementless Femoral Stem

Mamadou T. Bah<sup>a\*</sup>, Junfen Shi<sup>a</sup>, Markus O. Heller<sup>a</sup>, Yanneck Suchier<sup>b</sup>, Fabien Lefebvre<sup>b</sup>,  
Philippe Young<sup>c</sup>, Leonard King<sup>d</sup>, Doug G. Dunlop<sup>d</sup>, Mick Boettcher<sup>e</sup>, Edward Draper<sup>e</sup> and  
Martin Browne<sup>a</sup>

<sup>a</sup>Bioengineering Science Research Group, FEE, 5/3019, University of Southampton,  
Southampton SO17 1BJ, UK

<sup>b</sup>CETIM, Pôle Fatigue des Composants Mécaniques, 52, avenue Félix Louat - 60304 SENLIS  
Cedex, France

<sup>c</sup>Simpleware Ltd, Bradninch Hall, Castle Street, Exeter, EX4 3PL, UK

<sup>d</sup>Southampton University Hospitals NHS Trust, Tremona Road, Southampton, SO16 6YD,  
UK

<sup>e</sup>JRI Orthopaedics Ltd, 18 Churchill Way, 35A Business Park, Chapeltown, Sheffield, S35  
2PY, UK

**Keywords:** Short Stem; Primary Stability; Inter-subject Variability.

**Word count** (Introduction through acknowledgments): 3628 words

\*Corresponding Author:

Mamadou T. Bah

Bioengineering Science Research Group

Faculty of Engineering & the Environment

Room 5/3019

University of Southampton, Highfield

Southampton SO17 1BJ, UK

Tel.: +44 (0) 2380 592443

Fax: +44 (0) 2380 593016

Email: mtb@soton.ac.uk

### **Abstract**

This paper is concerned with the primary stability of the Furlong Evolution® cementless short stem across a spectrum of patient morphology. A computational tool is developed that automatically selects and positions the most suitable stem from an implant system made of a total of 48 collarless stems to best match a 3D model based on a library of CT femur scans (75males and 34 females). Finite Element contact models of reconstructed hips, subjected to physiologically-based boundary constraints and peak loads of walking mode, were simulated using a coefficient of friction of 0.4 and an interference-fit of 50µm. Maximum and average implant micromotions across the subpopulation were predicted to be 100±7µm and 7±5µm with ranges [15µm, 350µm] and [1µm, 25µm], respectively. The computed percentage of implant area with micromotions greater than reported critical values of 50µm, 100µm and 150µm never exceeded 14%, 8% and 7%, respectively. To explore the possible correlations between anatomy and implant performance, response surface models for micromotion metrics were constructed. Detailed morphological analyses were conducted and a clear nonlinear decreasing trend was observed between implant average micromotion and both the metaphyseal canal flare indices and average densities in Gruen zones. The present study demonstrates that the primary stability and tolerance of the short stem to variability in patient anatomy were high, reducing the need for patient stratification. In addition, the developed

tool could be utilised to support implant design and planning of femoral reconstructive surgery.

## **1. Introduction**

Cementless hip implants were initially designed to eliminate problems associated with the use of cement (Jasty et al., 1991). Notwithstanding good clinical results (Shah et al., 2009; Mannan et al., 2010), orthopaedists and engineers seek to continuously improve their geometries and promote implant stability through improved bone ongrowth and ingrowth around their surfaces (Wick and Lester, 2004; Sakai et al., 2008; Simpson et al., 2010). As a result, a wide range of contemporary cementless designs (polished, partially or fully coated ones, etc) and their respective clinical performances are well documented (Khanuja et al., 2011). There is still some debate, however, about the effect of long stems in terms of proximal femoral bone stock preservation and restoration, possible thigh pain and ease of implantation in the curved femoral canal, particularly for less experienced surgeons (Feyen and Shimmin, 2014). Shorter stem designs were introduced with the goal of maximising implant stability and conserving bone and soft tissue. A proximal lateral flare in shorter stems may reduce stress-shielding and produce a more physiological stress distribution. However, concerns exist about their primary torsional stability and such stems are not ideally suited to all patients due to the minimum area of healthy cancellous bone required for fixation (Renkawitz et al., 2008).

There is a consensus amongst the orthopaedic community that implant primary stability remains the major determinant in bone growth and the success of cementless THRs postoperatively (Pillar et al., 1986; Viceconti et al., 2006). Excessive bone-implant relative micromovements can compromise this stability (Pillar et al., 1986; Engh et al. 1992; Soballe et al., 1993). These micromovements depend on implant design and positioning (Howard et

al., 2004; Paratte et al., 2007; Andraus et al., 2008; Park et al., 2009; Dopico-González et al., 2010; Reggiani et al., 2008; Bah et al., 2011; Reimeringer et al., 2012), possible interfacial gaps and the magnitude of forces acting on the proximal femur and patient anatomy (Pancanti et al., 2003). Therefore, when introducing new stem designs, it is essential that rigorous pre-clinical testing is conducted, both computationally and physically, since clinical problems associated with new designs may not be evident for some time. Ideally, new stems should be tested in a wide range of patients, taking into account variability in anatomy, bone quality, implant positioning and loading. Experimental studies, although very useful for validation purposes, are often time consuming and would require an exhaustive number of bones. However, currently, studies often involve one or a few bones with one implant placed in a specific location and subjected to a specific load (Park et al., 2009; Pettersen et al., 2009; Østbyhaug et al., 2010; Harrison et al., 2014; Bieger et al., 2012).

Computational simulations have an advantage over experimental studies in that they allow parametric studies to be performed relatively easily e.g. by modifying loading, bone shape and quality. With faster computers and more advanced image processing softwares, more representative CT or MRI-based musculoskeletal models (Sigal et al., 2009; Baldwin et al., 2010; Vahdati et al., 2014; Martelli et al., 2014; Simpleware Ltd., 2014) can be now readily generated for analysis and micromotions along the entire implant surface can be predicted (Pancanti et al., 2003; Andraus et al., 2009; Park et al., 2009; Pettersen et al., 2009; Bah et al., 2011; Reimeringer et al., 2012; Fitzpatrick et al., 2014). In this respect, novel pre-clinical evaluation tools have been developed to: (a) enable the variability in patient geometry and bone quality using statistical shape modelling (Bryan et al., 2010; Blanc et al., 2012; Bah et al., 2013; Blanc et al., 2012; Rao et al., 2013; Fitzpatrick et al., 2014); (b) automatically assess the effects of implant positioning, loading, or bone-implant interface conditions for a specific patient (Abdul-Kadir et al., 2008; Bah et al., 2009; Dopico-González et al., 2010) or

(c) evaluate and compare the robustness of existing implant designs (Sakai et al., 2008; Reimeringer et al., 2012; Fitzpatrick et al., 2014).

To the authors' knowledge, no computational studies on the primary stability of cementless femoral stems using a wide range of CT-based patient specific 3D bone models have been reported yet in the literature (Viceconti et al., 2006; Bryan et al., 2012; Rao et al., 2013; Issa et al., 2014).

This paper explores the primary stability of a new short femoral stem design across a spectrum of patient morphology. Although, no clinical data are available for the considered stem design, it is questioned whether it will suit a wide range of patients in terms of acceptable levels of interfacial micromotions. It is also questioned what effects patient anatomy can have on stem performance. Hence, pre-clinical computational tools are developed that can be used to automatically select and position a stem for each specific patient, based on detailed morphological analyses. More importantly, the tools enable efficient analysis of implant primary stability across femoral morphologies and statistical correlation of patient anatomy with degree of implant micromotions. It is anticipated that the applications of these computational tools could form an essential first step towards robust design of new shorter cementless stems, which will involve modifying the geometric features of implants. Ultimately, the tools will help surgeons in selecting and positioning implants but also in improving their interaction with femur endosteal.

## **Methods**

### **Creation of Intact Femur Models**

A set of 109 3D femur models (75 male and 34 female, 43-106 years, voxel size: 0.488x0.488x1.5mm-0.7422x0.7422x0.97mm) were generated from slices obtained from CT scan data, following manual segmentation of cross sectional images using ScanIP software

(Simpleware Ltd., UK). The average weight, average height and BMI for females were  $73.02 \pm 11.93$  kg,  $1611 \pm 65.83$  mm and  $28.19 \pm 4.78$  kg.m<sup>2</sup>, respectively compared to  $88.07 \pm 16.5$  kg,  $1773.5 \pm 98.29$  mm and  $27.89 \pm 3.92$  kg.m<sup>2</sup> for males. The material properties were automatically assigned in ScanIP, assuming a linear relationship between the apparent density of the bones ( $\rho$ ) and the Hounsfield unit from the CT scan. The elastic modulus of bone to apparent density relationship was of the form  $E = 6850\rho^{1.49}$  (Morgan et al., 2003), based on reported results of Schileo et al. (2007), following a numerical-experimental study of the effects of density–elasticity relationships on the amount of strain generated in long bones such as femurs (Schileo et al.; (2007)). Finite elements within the medullary canal had a density of  $0$  g/cm<sup>3</sup> while a peak value of  $1.73$  g/cm<sup>3</sup> was assigned to the densest cortical bone of the femoral shaft (Bryan et al., 2010). For each of the reconstructed CT-based femur model a total of 22 parameters were employed to describe the anatomy (Bah et al., 2013): 7 periosteal and 8 endosteal including femoral canal flare indices and average densities in 7 Gruen zones, see Appendix A for more details.

### **Femur Implantation and Finite Element Contact Analysis**

The cementless FURLONG EVOLUTION® collarless titanium alloy ( $E=105$ GPA,  $\nu=0.3$ ) femoral short stem design (JRI Orthopaedics Ltd, UK) was used in this study. The  $126^\circ$  or  $133^\circ$  CCD angle stem, with either a low or high offset, has a distal size ranging from 6 to 17mm; this forms a full implant system of 48 stems. Table 1 shows the values of 7 geometrical parameters defined for each of the 12 available stems available for this study. The optimal implant configuration (CCD angle, femoral offset, neck length, canal width) and size were automatically selected to best approximate the 3D morphology of each femur. To this end, a script was developed that first compared CCD angles, neck lengths and offsets of both femur and stem but also minimised the difference between the femur canal width (2cm

above the lesser trochanter) against the stem proximal width. The stem was placed such that its axes matched those of the femoral shaft and neck. Finally, the stem was positioned such that the distance between centers of femoral and implant heads was minimum. Figure 1 displays the process of automated anatomic measurement and implant selection and match process.

Another script was developed that can automatically export the bone and stem geometries to +CAD software (Simpleware Ltd., UK) for Boolean operations and generation of the reconstructed hip. Note that for each specific stem, a unique cutter was used for removal of the head and creation of the femoral cavity. The implanted femur was then meshed in ScanIP (Simpleware Ltd., UK) using tetrahedral elements, see Table A1 in Appendix A for meshing parameters. A typical mesh contained 68050 nodes and 284155 elements for the bone and 20510 nodes and 81425 elements for the implant. A mesh quality inspection was also performed to make sure that all elements were well shaped, i.e. the limit values of metrics such as in-out aspect ratio (0.02), edge length ratio (20), angular/volume skew (1/0.99), shape factor (0.01%), minimum dihedral angle (2), maximum dihedral angle (177), jacobian (0.019) or minimum edge length (0.01) were not violated. The mesh settings resulted in stem average micromotions comparable to those obtained by Reimeringer et al. (2012). Node-to-node correspondence at the bone-implant interface was achieved and contact surface pairs and node sets for application of boundary conditions and loading were automatically created. A third script read each implanted femur mesh into Ansys 14.5 (Ansys Inc., 2014) for frictional contact analysis using a coefficient of friction of 0.4 and an interference fit of 50 $\mu$ m (Abdul-Kadir et al., 2008), see Appendix B for more details on contact analysis. Each model was subjected to physiological displacement constraints (Speirs et al., 2008) and peak joint/muscle forces during walking (HIP98 data, [www.orthoload.com](http://www.orthoload.com)), scaled to each patient anatomy, to determine bone-implant interface mechanics. Joint forces were applied at the

head centre and 8 muscle forces (Heller et al., 2005) were mapped and distributed to subsets of nodes, each subset corresponding to target nodes attached to elements sharing the closest node to the muscle force application point.

### **Postprocessing of Implant Micromotion**

For efficient analysis of implant primary stability and distributions of intra and inter-patient micromotion distributions, the following metrics were processed: average micromotion; maximum micromotion and percentage of implant area with micromotions greater than reported bone growth threshold limits of 50 $\mu\text{m}$  (Szmukler-Moncler et al., 2000), 100 $\mu\text{m}$  and 150 $\mu\text{m}$  (Soballe et al., 1993). These percentages will be referred to as PIAM50, PIAM100 and PIAM150, respectively. Linear fits between metrics and anatomy parameters were attempted and coefficients of determination of fit were calculated. Finally, the effects of 22 measured femoral anatomy parameters (15 geometrical and 7 Gruen zones average densities) and implant design parameters on implant micromotion metrics were investigated in a statistical sense. Note that for each of the 109 finite element models considered in this work, each node was associated with a unique density value. Therefore, for each of the 7 Gruen zones, the average density was computed by simply dividing the total density over all nodes in the zone by the total number of nodes. The set of processed micromotion metrics were therefore used to construct surrogate models for each metric using “Kriging”, a regression methodology based on Bayesian processes (Deutsch and Journel, 1992; Rasmussen and Williams, 2006; Bah et al., 2011) that is particularly suitable for highly nonlinear responses and optimisation studies. Correlation charts were drawn to measure the possible correlation between considered anatomy and implant design parameters and micromotion metrics using modeFRONTIER multi-objective and multi-disciplinary optimization software. Finally, sensitivity analysis was conducted to identify the most influential patient-related parameters on implant primary stability and to isolate the least influential ones.

### 3. Results

Table 2 shows the mean and standard deviation of measured anatomical parameters that were used for selection and positioning of stem designs. The highest standard deviations were found in the vertical and medial offsets and CCD angle. The application of the ‘‘stem positioning’’ script revealed that that 7 out of 12 stem designs were automatically selected for the 109 considered femurs: a 126° CCD stem with low offset (sizes 12 and 13) and high offset (size 13); and a 133° CCD stem with low offset only (sizes 6, 12 and 17). The stem design that fitted most femurs (36 male and 20 female) was 33mm wide with a 126° CCD angle, a medial offset of 40.9mm, a vertical offset of 26.4mm and a 13mm distal stem diameter.

The FE simulations revealed that during walking, the maximum and average implant micromotions across the subpopulation were  $100\pm 7\mu\text{m}$  and  $7\pm 5\mu\text{m}$  with ranges  $[15\mu\text{m}, 350\mu\text{m}]$  and  $[1\mu\text{m}, 25\mu\text{m}]$ , respectively. Overall, high micromotions were found medially and were greatest in femurs with the lowest bone density in over 100 reconstructions. To illustrate this, three patients aged 47 (Patient 1), 37 (Patient 2) and 83 years (Patient 3) were selected. Table 3 details patient anatomy and stem parameters. All femurs were implanted with a 126° CCD angle and standard offset stem with a distal size of 11mm for Patient 1 and 13mm for Patients 2&3. Note that the overall bone density and canal flare indices were higher for Patient 1, followed by Patient 3 and 2. The resulting average and maximum micromotions were  $1\mu\text{m}$  and  $17\mu\text{m}$ ,  $10\mu\text{m}$  and  $283\mu\text{m}$ ,  $25$  and  $164\mu\text{m}$ , respectively. Figure 3 displays micromotion distributions for all three patients. The computed percentage of stem areas with different micromotion levels revealed that across all patients PIAM50, PIAM100 and PIAM150 never exceeded 14%, 8% and 7%, respectively.

To explore the possible variability in the distribution of implant micromotion across the population due to changes in bone quality and shape, patients were divided by gender, selected anatomy parameters and stem sizes. First, PIAM50, PIAM100 and PIAM150 were used for comparison of micromotion distribution between: females and males, the 126° and 133° CCD stems; the 12mm and 13mm stem sizes. No significant differences were found between males and females or between femurs implanted with different stems. The percentages of implant area decreased with bone growth threshold values and were always higher when interference was taken into account (Figure C1 in Appendix C). When these percentages were plotted separately against each of the considered patient and stem design parameters, no clear trends were found (Figure C2 in Appendix C).

When the average micromotion metric was used, a clearer trend was observed for two parameters: the metaphyseal canal flare index measured in medial-lateral (ML MCFI), neck-oriented (NO MCFI) and ante-posterior directions (AP MCFI) and the average bone density in the seven Gruen zones (Figures 4 and 5). All other parameters didn't show any clear effect on the average micromotion (Appendix D). Reduced metaphyseal CFIs (Figure 4) and mean density in the seven Gruen zones (Figure 5) were associated with a nonlinear increase in the average micromotions of the short cementless implant in over 100 femoral reconstructions. Linear fits of the data revealed that 14%, 19% and 17.5% of the average micromotion can be explained by a linear combination of ML MCFI, AP MCFI and NO MCFI, respectively. Similarly for bone density, these coefficients were 18%, 23.3%, 23.6%, 20%, 21%, 19.8% and 24% for Gruen zone 1 to Gruen zone 7.

Traditionally, femoral shapes are classified into three types, using the CFI index (Noble et al., 1988): stovepipe ( $CFI < 3$ ), normal ( $3 < CFI < 4.7$ ) and champagne-flute ( $4.7 < CFI < 6.5$ ). Plotting the standard CFIs against the metaphyseal CFIs (Figure 6) revealed that the limit values of 3 and 4.7 for the ML CFI corresponds approximately to 2 and 3 for the ML MCFI,

i.e. average micromotions of around 10 $\mu$ m and 3 $\mu$ m, respectively (Figure 4). Similarly for AP MCFI and NO MCFI, the limit values were [1.5, 2] and [2, 2.8]. The proximal femur was further classified, based on revealed effects of Gruen zone densities on implant average micromotion. On the medial side, the micromotion thresholds of 10 $\mu$ m and 3 $\mu$ m correspond to the following density limit values: zone 1 (0.3-0.7g/cm<sup>3</sup>), zone 2 (0.6-0.9g/cm<sup>3</sup>), zone 3 (0.75-1.1g/cm<sup>3</sup>). Similarly, on the lateral side: zone 5 (0.8-1.2g/cm<sup>3</sup>), zone 6 (0.5-1g/cm<sup>3</sup>), zone 7 (0.4-0.85g/cm<sup>3</sup>). Finally, for zone 4, density limit values are 0.8-1.2 g/cm<sup>3</sup>.

In the rest of the analysis, the average micromotion data was fitted into a Kriging-based surrogate model. The calculation of the coefficients of determination of linear fit revealed that a maximum of 25.6%, 28.5% and 27.7% of average micromotion can be explained by a linear combination of ML MCFI, AP MCFI and NO MCFI, respectively. Similarly for bone density, these coefficients were 27%, 35%, 37%, 36%, 30%, 32% and 35% for Zones 1-7. Figure 7a summarises a correlation chart together with graphs showing the dependence between all parameters. The sensitivity analysis results (Figure 7b) revealed that all parameters, metaphyseal canal flare indices and bone densities had a comparable importance on the changes in implant average micromotion.

#### **4. Discussions**

This paper explored the primary stability of a cementless short hip stem across varied patient morphology. Simulations revealed that, across all patients, the implant average micromotion never exceeded 25 $\mu$ m. The largest areas with micromotions greater than 50  $\mu$ m were found on the posterior side towards the medial region of the stem but never exceeded 14% of the total implant-bone contact area. This suggest that the implant primary stability and the tolerance to subject variability were high, meaning that the short stem would not reduce the shear strength at the bone-implant interface or drastically reduce the ability to transfer applied loads to the surrounding bone.

The load was well distributed, especially on the medial and lateral and posterior sides of the proximal bone as illustrated in three selected patients of different age, morphology and bone quality (Figure 3). As the micromotion limit value was increased to 100 $\mu$ m and 150 $\mu$ m, the computed implant percentage area decreased to 8% and 7%, respectively. No significant differences were found between females and males in terms of this percentage area. The effects of interference-fit were also clearly captured by an increase in micromotion compared to the no interference-fit condition. No clear trends were found between these percentages and patient anatomy or stem design parameters.

The present study revealed that the average micromotion across the population nonlinearly decreased with both the 3D metaphyseal canal flare indices (MCFI) and Gruen zone bone densities (Figures 4 and 5). Other parameters such as the standard canal flare index (Noble et al., 1988) that have been widely used for classification of the proximal femur, neck length or patient mass did not show a clear influence on the short stem average micromotion. For short stems, a new classification of the proximal femur was attempted using linear fits between standard and metaphyseal CFIs (Figure 6) This might help to pre-define osteoporotic osteoarthritic and normal canal patients but also to maximise the bone-implant contact area in the metaphyseal region (lower the level of generated micromotions).

Fitting the average micromotion data into a Kriging-based surrogate model revealed that a maximum change of around 27% (on average) in micromotion could be explained by MCFI indices and around 33% by Gruen zone densities. The correlation chart in Figure 7a clearly shows the dependence strength between anatomy parameters and average micromotion and the relative importance of each parameter in possible micromotion changes across patients. This might confirm that the metaphyseal filling together with a good fit between a short stem and the proximal bone are crucial in assuring postoperative initial implant stability as this

maximises the percentage of transmitted applied forces to the metaphysis and not to the diaphysis (Jasty et al., 1994; Santori et al., 2006; Santori and Santori, 2010).

There is still some debate on the use of short stems and their ability to achieve immediate postoperative stability (Renkawitz et al., 2008; Shah et al., 2009; Santori and Santori, 2010; Khanuja et al., 2011; Bieger et al., 2012). It is believed that young and active patients would benefit from their use. At the same time, it is clear that apart from implant design selection and materials or surgical procedures, patient anatomy and bone quality are key factors in the outcome of successful surgery. The cementless short stem designs considered here showed a high primary stability across patients and the possible level of micromotions can be controlled by the metaphyseal canal flare indices together with accurate measurements of bone densities. This study therefore supports that if the short stem is well placed in the metaphyseal region of the proximal femur, a good stability can be predicted even for osteoporotic-type patients.

The clinical relevance of reported micromotions and the effects of inter-patient variability on implant primary stability is subject to interpretation in the absence of long term follow-up clinical data for the relatively recent stem considered here (Feyen and Shimmin, 2014). However, a main aim of the present analysis was to capture the critical micromotion levels that might occur at peak loads when both implant and bone surfaces slip under frictional and interference-fit conditions. Another aim was to effectively capture the effects of variability in femoral morphologies on the possible scatter and distribution of implant micromotions.

The presented results would suggest that patient stratification is not necessary for the considered short cementless stem. Further analyses, using a standard long stem design and/or under more challenging musculoskeletal loading conditions, are required to confirm reported results as the magnitude of micromotion depends on the magnitude of forces applied to the

proximal femur. It is also envisaged to apply the proposed pre-clinical tools to a wider range of patients or target a specific subgroup of interest (for example those of poor bone quality and low metaphyseal canal flare indices) by exploring statistical shape and intensity modelling of bones. It is anticipated that these tools will assist surgeons in making a better decision when selecting and positioning implants but also in choosing the surgical procedure.

**Conflict of interest**

All authors declare that they have no conflict of interest.

**Acknowledgements**

The authors would like to acknowledge Cetim (Research Contract 12028/01-RP009755), the EPSRC Impact Acceleration Account (IAA) Knowledge Transfer Secondments UK for supporting this research (Grant Number EP/E057705/1), for Southampton University General Hospital for providing patient CT scans and JRI Orthopaedics Ltd (Sheffield, UK) for supplying Furlong Evolution® femoral stems.

## References

Andreas, U., Colloca, M., Toscano A., 2008. Mechanical behaviour of a prosthesised human femur: a comparative analysis between walking and stair climbing by using the finite element method. *Biophysics and Bioengineering Letters* 1(3), 1-15, ISSN: 2037-0199.

Andreas, U., Colloca M., 2009. Prediction of micromotion initiation of an implanted femur under physiological loads and constraints using the finite element method. *Procs. of the Inst. of Mechanical Engineers Part H, J. of Engineering in Medicine* 223(5), 589-605.

ANSYS, 2013. ANSYS Theory Reference Manual Release 14.5, Ansys Inc.

Abdul-Kadir, M.R., Hansen, U., Klabunde, R., Lucas, D., Amis, A., 2008. Finite element modelling of primary hip stem stability: The effect of interference fit. *Journal of Biomechanics* 41(3), 587-594.

Bah, M. T., Shi, J. Browne, M., Suchier, Y. Lefebvre, F., Young, P., King, L., Dunlop, D., M. O. Heller, 2013. Gender-Specific Statistical Shape Model of the Femur for Automated Image-Based Anatomic Parameter Measurements. *J. Bone Joint 95-B Supp* 34, 233.

Bah, M.T., Nair, P.B., Taylor, M., Browne, M., 2011. Efficient computational method for assessing the effects of implant positioning in cementless total hip replacements. *Journal of Biomechanics* 44 (7), 1417–1422.

Bah, M.T., Nair, P.B., Browne, M., 2009. Mesh morphing for finite element analysis of implant positioning in cementless total hip replacements. *Medical Engineering & Physics* 31(10), 1235-1243.

Barrack, R.L., 2003. Dislocation after total hip arthroplasty: implant design and orientation. *Journal of the American Academy of Orthopaedic Surgeons* 11(2), 89-99.

Bergman, G., Deuretzbacher, G., Durselen, L., Pohl, M., Claes, L., Hass, M.P., Duda, G.N., 2001. Muskulo-skeletal loading conditions at the hip during walking and stair climbing. *Journal of Biomechanics* 34, 883-893.

Bieger, R., Ignatius, A., Decking, R., Lutz, C., Reichel, H., Dürselen, L., 2012. Primary stability and strain distribution of cementless hip stems as a function of implant design *Clinical Biomechanics* 27(2), 158-164.

Bryan, R., Mohan, P.S., Hopkins, A., Taylor, M., Nair, P.B., 2010. Statistical modelling of the whole human femur incorporating geometric and material properties, *Medical Engineering and Physics* 32(1), 57-65.

Bryan, R., Nair, P.B., Taylor, M., 2012. Influence of femur size and morphology on load transfer in the resurfaced femoral head: A large scale, multi-subject finite element study. *Journal of Biomechanics* 45(11):1952-1958.

Bergman, G., Deuretzbacher, G., Durselen, L., Pohl, M., Claes, L., Hass, M.P., Duda, G.N., 2001. Muskulo-skeletal loading conditions at the hip during walking and stair climbing. *Journal of Biomechanics* 34, 883-893.

Dopico-González, New, A.M, Browne, M., 2010. Probabilistic finite element analysis of the uncemented hip replacement—effect of femur characteristics and implant design geometry. *Journal of Biomechanics* 43(3), 512-520.

Engh, C.A., O'Connor, D., Jasty, M., McGovern, T.F., Bobyn, J.D. and Harris W.H., 1992. Quantification of implant micromotion, strain shielding, and bone resorption with porous-coated anatomic medullary locking femoral prostheses. *Clin. Orthop.* 285, 13–29.

Feyen, H., and Shimmi, A.J., 2014. Is the length of the femoral component important in primary total hip replacement? Is the length of the femoral component important in primary total hip replacement ? *J. Bone Joint* 96-B, 442-448.

Fitzpatrick, C.K., Hemelaar, P. and Taylor, M., 2014. Computationally efficient prediction of bone-implant interface micromotion of a cementless tibial tray during gait. *Journal of Biomechanics* 47(7), 1718-1726.

Gruen, T.A., McNeice, G.M., Amstutz, H.C., 1979. Modes of failure of cemented stem-type femoral components: a radiographic analysis of loosening. *Clinical Orthopaedics* 141, 17-27.

Grubl, A., 2002. Cementless total hip arthroplasty with a tapered rectangular titanium stem and a threaded cup a minimum ten-year follow-up. *The Journal of Bone and Joint Surgery* 84A(3), 425-431.

Harrison N., Field J.R., Quondamatteo, F., Curtin, W., McHugh, P.E., Mc Donnell, P., 2014. Preclinical trial of a novel surface architecture for improved primary fixation of cementless orthopaedic implants. *Clinical Biomechanics*. DOI: 10.1016/j.clinbiomech.2014.07.007.

Heller, M.O., Bergmann, G., Kassi, J.-P., Claes, L., Haas, N.P., Duda, G.N., 2005. Determination of muscle loading at the hip joint for use in pre-clinical testing. *Journal of Biomechanics* 38(5), 1115-1163.

Howard, J.L., Hui, A.J., Bourne, R.B., McCalden, R.W., MacDonald, S.J., Robareck, C.H., 2004. A quantitative analysis of bone support comparing Cementless tapered and distal fixation total hip replacements. *The Journal of Arthroplasty* 19(3), 266-273.

Issa, K., Stroh, A.D., Mont, M.A. and Bonutti, P.M., 2014. Effect of Bone Type on Clinical and Radiographic Outcomes of a Proximally-Coated Cementless Stem in Primary Total Hip Arthroplasties. *Journal of Orthopaedic Research*. DOI: 10.1002/jor.22648.

Jasty, M., O'Connor, D.O., Henshaw, R.M, et al., 1994. Fit of the uncemented femoral component and the use of cement influence the strain transfer the femoral cortex. *J Orthopaedic Research* 12, 648–56.

Jasty, M., Maloney, W. J., Bragdon, C. R., O'Connor, D. O., Haire, T., and Harris, W. H., 1991. The Initiation of Failure in Cemented Femoral Components of Hip Arthroplasties. *J. Bone Joint Surg. Br.* 73B, 551–558.

Khanuja, H.S., Vakil, J.J., Goddard, M.S. and Mont, M.A., 2011. Cementless Femoral Fixation in Total Hip Arthroplasty. *J Joint Surg Am.* 93, 500-509.

Rao, C, Fitzpatrick, C.K, Rullkoetter, P.J., Maletsky, L.P., Kim, R.H., Laz, P.J., 2013. A statistical finite element model of the knee accounting for shape and alignment variability. *Medical Engineering Physics* 35(10), 1450-1456.

Blanc R, Seiler C, Szekely G, Nolte L-P, Reyes, M. 2012. Statistical model based shape prediction from a combination of direct observations and various surrogates: Application to orthopaedic research 16: 1156–1166.

*Mannan*, K., Freeman, M.A.R. and Scott, G. 2010. *J. Bone Joint Surgery* 92B(4), 480-485.

Pancanti, A., Bernakiewicz, M., Viceconti, M., 2003. The primary stability of a cementless stem varies between subjects as much as between activities. *Journal of Biomechanics* 36, 777-785.

Martelli, S., Valente, G., Viceconti, M., Taddei, F., 2014. Sensitivity of a subject-specific musculoskeletal model to the uncertainties on the joint axes location. *Computer Methods in Biomechanics and Biomedical Engineering*. DOI: 10.1080/10255842.2014.930134.

Morgan, E.F., Bayraktar, H.H., Keaveny, T.M., 2003. **Trabecular bone modulus-density relationships depend on anatomic site.** *Journal of Biomechanics* 36(7): 897-904.

Noble, P.C., Jerry, W., Alexander, J.W., Lindhal, L.J., Yew, D.T. and Granberry, W.M., 1988. The anatomical basis of femoral component design. *Clin Orthop* 235, 148–65.

Østbyhaug, P.O., Klaksvik, J. Romundstad, P. and Aamodt, A., 2011. Primary stability of custom and anatomical uncemented femoral stems. A method for three-dimensional in vitro measurement of implant stability. *Clin. Biom.*25, 318-324.

Park, Y., Choi, D., Hwang, D.S., and Yoon, Y-S., 2008. Primary stability of cementless stem in THA improved with reduced interfacial gaps. *Journal of Biomechanical Engineering* 130, 1-7.

Parratte, S., Argenson, J.-N.A., 2007. Validation and usefulness of a computer-assisted cup-positioning system in total hip arthroplasty. *The Journal of Bone & Joint Surgery* 89-A, 494-499.

Pettersen, S. H., Wik, T. S., Skallerud, B., 2009. Subject specific finite element analysis of implant stability for a cementless femoral stem. *Clinical Biomechanics* 24, 480-487.

Pillar, R.M., Lee, J.M., Maniopoulos, C., 1986. Observation on the effect of movement on bone ingrowth into porous-surfaced implants. *Clin. Orthop. Relat. Res.* 20, 108-113.

Rasmussen, C.E. and Williams, C.K.I., 2006. *Gaussian processes for Machine Learning*-MIT Press.

**Reggiani, B., Cristofolini, L., Taddei, F., and Viceconti, M., 2008. Sensitivity of the primary stability of a cementless hip stem to its position and orientation. *Artificial Organs* 32(7), 555-560.**

- Reimeringer, M., Nuño, N., Desmarais-Trépanier, C. Lavigne, M. and Vendittoli, P.A. 2012. The influence of uncemented femoral stem length and design on its primary stability: a finite element analysis. *Computer Methods in Biomechanics and Biomedical Engineering* 16(11), 1-11.
- Renkawitz, T., Santori, F.S., Grifka, J., Valverde, C., Morlock, M.M. and Learmonth, I.D., 2008. A new short uncemented, proximally fixed anatomic femoral implant with a prominent lateral flare: design rationals and study design of an international clinical trial. *BMC Musculoskeletal Disorders* 9, 1-6.
- Rohlmann, A, Cheal, E.J., Hayes, W.C., Bergman, G., 1988. A Non-linear finite element analysis of interface conditions in porous-coated hip endoprostheses. *Journal of Biomechanics* 36, 1079-1086.
- Ruben, R. B., Folgado, J. and Fernandes, P.R., 2007. Three-dimensional shape optimization of hip prostheses using a multicriteria formulation. *Structural and Multidisciplinary Optimization* 34(3), 261-275.
- Sakai, T., Ohzono, T., Nishii, T., Miki, H., Takao, M. and Sugano, N., 2010. A modular femoral neck and head system works well in cementless total hip replacement for patients with developmental dysplasia of the hip. *J Bone Joint Surg Br.* 92B, 770-776.
- Santori F.S., Manili, M., Fredella, N., et al., 2006. Ultra short stems with proximal load transfer: Clinical and radiographic results at five year follow-up. *Hip Int.* 16(Suppl 3), 31-39.
- Santori, F.S. and Santori, N., 2010 Mid-term results of a custom-made short proximal loading femoral component. *J Bone Joint Surg Br.* 92(9), 1231-1237.
- Santori, N, Albanese, C.V., Learmonth, I.D. and Santori, F.S. 2006. Bone preservation with a conservative metaphyseal loading implant. *Hip Int.* 16 (Suppl 3):16-21.

Simon, U, Augat, P., Ignatius A., Claes, L., 2003. Influence of the stiffness of bone defect implants on the mechanical conditions at the interface – a finite element analysis with contact. *Journal of Biomechanics* 36, 1079-1086.

Shah, N.N., Edge A.J., and Clark D.W., 2009. Hydroxyapatite-ceramic-coated femoral components in young patients followed-up for 16 to 19 years. *J Bone Joint Surg Br.* 91B, 865–869.

Schileo, E., Taddei, F., Malandrino, A., Cristofolini, L. and Viceconti, M., 2007. Subject-specific finite element models can accurately predict strain levels in long bones. *Journal of Biomechanics* 40(13), 2982–2989.

Simpleware Ltd., ScanIP, +CAD, +NURBS software version 6.0 reference guide. Exeter, UK, 2014 (<http://www.simpleware.com>).

Simpson, D.J., Kendrick, B.J.L., Hughes, M., Glyn-Jones, S., Gill, H.S., Rushforth, G.F. and Murray, D.W., 2010. The migration patterns of two versions of the Furlong cementless femoral stem. A randomised, controlled trial using radiostereometric analysis. *J Bone Joint Surg.* 92B, 1356-1362.

Soballe, K., Hansen, E.S., Brockstedt Rasmussen, H., Bunger, C., 1993. Hydroxyapatite coating converts fibrous tissue to bone around loaded implants. *Journal of Bone and Joint Surgery. British Volume* 75, 270–278

Speirs, A.D., Heller, M.O., Duda, G.N. and Taylor W.R., 2007. Physiologically based boundary conditions in finite element modelling. *Journal of Biomechanics* 40(10), 2318-2323.

Stolk J., Verdonschot, N., Huiskes, R., 1998. Sensitivity of failure criteria of cemented total hip replacements to finite element mesh density. *Journal of Biomechanics* 30, 165.

Sumner, D.R., Turner, T.M., Igloria, R., Urban, R.M., Galante, J.O., 1998. Functional adaptation and ingrowth of bone vary as a function of hip implant stiffness. *Journal of Biomechanics* 31, 909-917.

Taddei, F., Pancanti, A., Viceconti, M., 2004. An improved method for the automatic mapping of computed tomography numbers onto finite element models, *Journal of Medical Engineering & Physics* 26, 61-69.

Vahdati, A., Walscharts, S., Jonkers, I., Garcia-Aznar, J.M., Vander Sloten, J., van Lenthe, J.H., 2014. Role of subject-specific musculoskeletal loading on the prediction of bone density distribution in the proximal femur. *Journal of the Mechanical Behaviour of Biomedical Materials* 30, 244-252.

Viceconti, M., Muccini, R., Bernakiewicz, M., Baleani, M., Cristofolini, L., 2000. Large-sliding contact elements accurately predict levels of bone-implant micromotion relevant to osseointegration. *Journal of Biomechanics* 33, 1611-1618.

Viceconti, M., Brusi, G., Pancanti, A., Cristofolini, L., 2006. Primary stability of an anatomical cementless hip stem: A statistical analysis. *Journal of Biomechanics* 39(7), 1169-1179.

Weinans, H., Sumner, D.R., 1997. Finite element analysis to study periprosthetic bone adaptation. In: Lowet, G., Ruegsegger, P., Weinans, H., Meunier, A. (Eds), *Bone research in biomechanics*. IOS Press, Amsterdam, pp. 3-16.

Wick, M. and Lester, D.K., 2004. Radiological changes in second- and third-generation Zweymüller stems. *J Bone Joint. Surg.* 86B, 1108-1114.

## List of Tables:

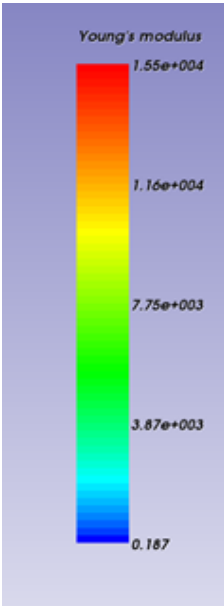
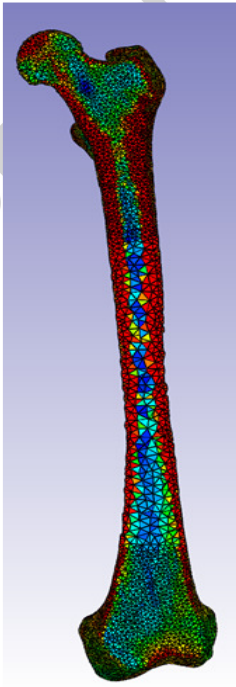
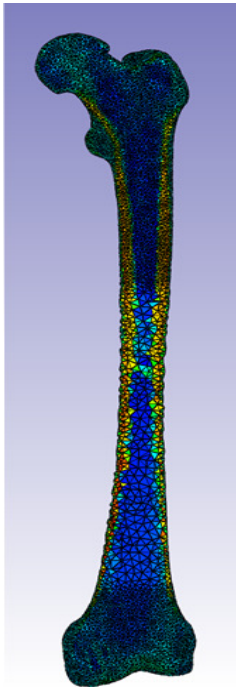
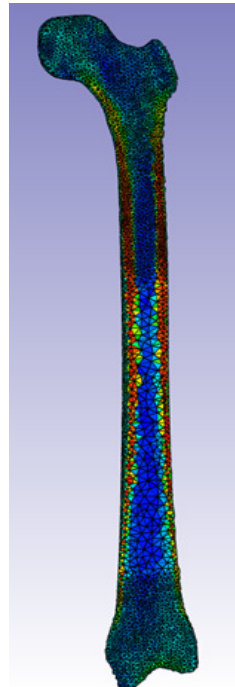
**Table 1: FURLONG EVOLUTION Short Cementless Stem Design Parameters.**

CCD angle, °	Neck Length, mm	Neck Offset, mm		Stem Proximal Width, mm	Stem Distal Size, mm	Stem Length, mm
		Medial	Vertical			
126	31.6	40.9	26.4	31, 32, 33	11, 12, 13	100
	35.3	45.9	26.4	31, 32, 33	11, 12, 13	100
133	32	36.9	31	23, 32, 37	6, 12, 17	100
	35.7	41.9	31	23, 32, 37	6, 12, 17	100

**Table 2: Mean and standard deviation of selected femoral parameters.**

Measured Parameter	Mean and Standard Deviation	
	Female	Male
maximum femur length (MFL), mm	432.41±17.53	475.29±26.96
maximum femoral head diameter (FHD), mm	43.5±1.3	45.8±1.5
femoral neck length (FNL), mm	48.8±3.5	51.27±5
femoral head medial offset (HMO), mm	38.21±3.28	40.43±4.61
femoral head vertical offset (HMO)	55.78±6.4	65.11±7.29
collo-diaphyseal angle (CCD), °	124.9±5.2	126.3±4.6
anteversion angle, °	13±6.4	6.3±7.8
isthmus position, mm	104.27±20.81	99.60±26.93
cortical thickness at isthmus, mm	7.56±1.29	8.54±1.05
ML canal flare index (ML CFI)	4.13±0.55	4.03±0.66
AP canal flare index (AP CFI)	1.91±0.31	1.88±0.44
NO canal flare index (NO CFI)	3.77±0.58	3.78±0.63
ML metaphyseal CFI (ML MCFI)	2.31±0.32	2.31±0.34
AP metaphyseal CFI (AP MCFI)	1.61±0.29	1.69±0.30
NO metaphyseal CFI (NO MCFI)	2.35±0.33	2.30±0.35
Gruen Zone 1 average density, g/cm <sup>3</sup>	0.38±0.14	0.44±0.17
Gruen Zone 2 average density, g/cm <sup>3</sup>	0.64±0.18	0.72±0.17
Gruen Zone 3 average density, g/cm <sup>3</sup>	0.80±0.16	0.91±0.18
Gruen Zone 4 average density, g/cm <sup>3</sup>	0.91±0.17	1.02±0.18
Gruen Zone 5 average density, g/cm <sup>3</sup>	0.85±0.18	0.95±0.18
Gruen Zone 6 average density, g/cm <sup>3</sup>	0.60±0.18	0.70±0.20
Gruen Zone 7 average density, g/cm <sup>3</sup>	0.49±0.16	0.57±0.21

**Table 3: Anatomy parameters of selected patients and stems for direct comparison of micromotion distribution.**

Parameters	Patient 1	Patient 2	Patient 3
Gender	Male	Male	Female
Age, years	47	37	83
Weight, kg	60.37	80.94	87.45
CCD angle, °	127.4	123.5	124.48
Femoral head offset, mm	40.25	42.16	41.08
Femoral neck length, mm	51.12	49.39	50.61
Canal Thickness (mm) – 2mm above the lesser trochanter	38.27	47.94	52.82
Anteversion (°)	7.98	-2.13	7.55
ML CFI	4.83	3.73	4.57
ML MCFI	2.69	1.97	1.99
Stem CCD angle, °	126	126	126
Stem Medial Offset, mm	40.9	40.9	40.9
Stem Width, mm	31	33	33
Stem Distal Size, mm	11	13	13
 <p>Young's modulus (MPa) Distribution</p>			

## Figure Legends:

Figure 1: Automated Anatomic Measurement and Implant Selection and Match Process.

Figure 2: Top plot shows a typical finite element mesh of an implanted femur model. Bottom plot shows distributed forces (hip contact, abductor, tensor fasciae latae and vastus lateralis) and constrained nodes (hip centre deflects along an axis towards the knee centre fixed in all directions and the distal lateral epicondyle constrained in y-direction to prevent rigid body motion (Speirs et al., 2007)).

Figure 3: Anterior (left) and posterior (right) view of a typical implant micromotion distribution in three selected patients: two male patients aged 47 (top) and 37 (middle) years and in one female patient aged 83 (bottom). Grey areas correspond to micromotions over 50  $\mu\text{m}$ .

Figure 4: Changes of average micromotion against metaphyseal canal flare index. Females (red), Males (blue). Same legend as in Figure 5. Females (red), Males (blue). 426 and 433 refer to 126° and 133° CCD angle; 02 and 52 refer to standard (40.9mm) and high (45.9mm) neck offset; 11, 12, 13, 17 refer to stem distal size (mm).

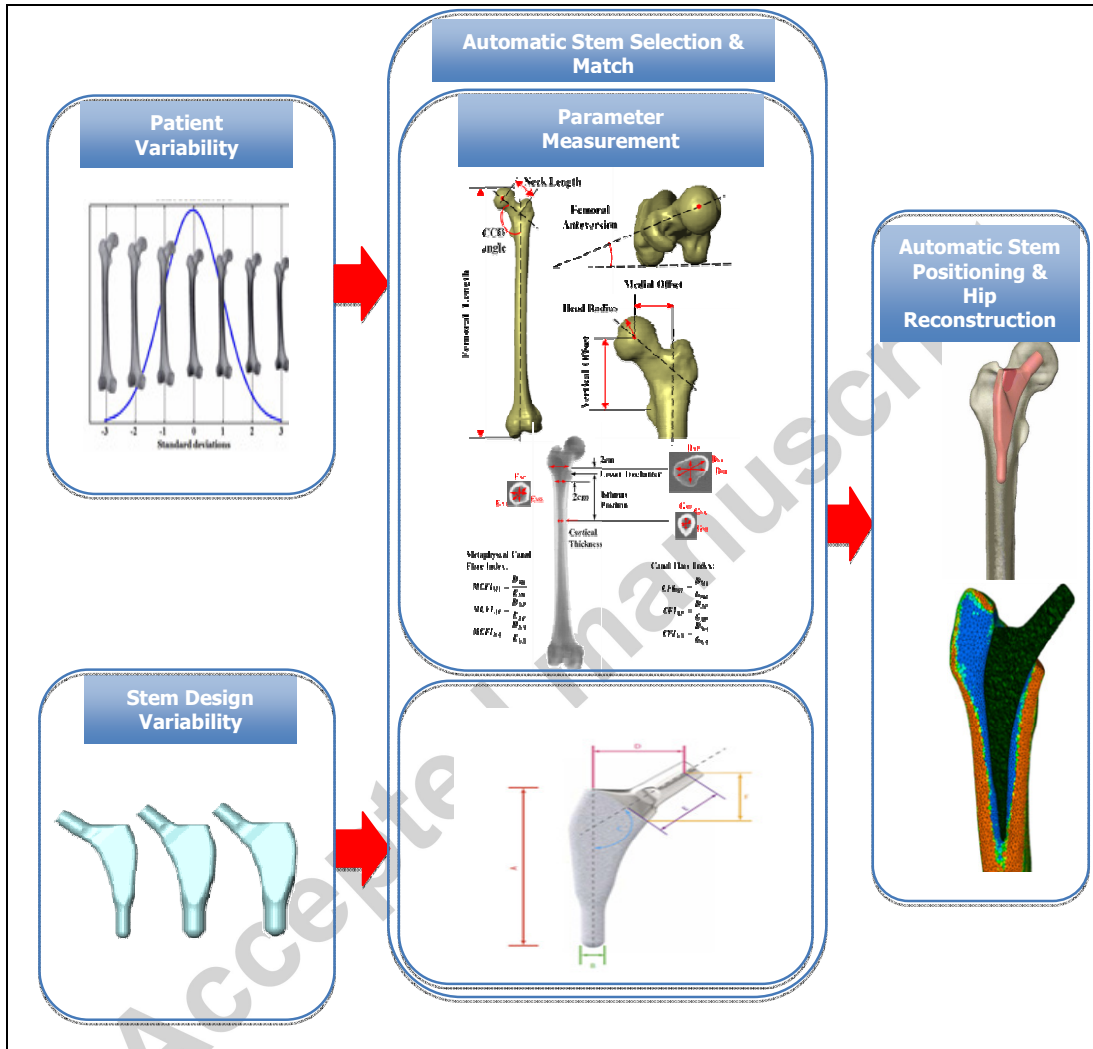
Figure 5: Changes of average micromotion against mean density in Gruen zones. Same legend as in Figure 3.

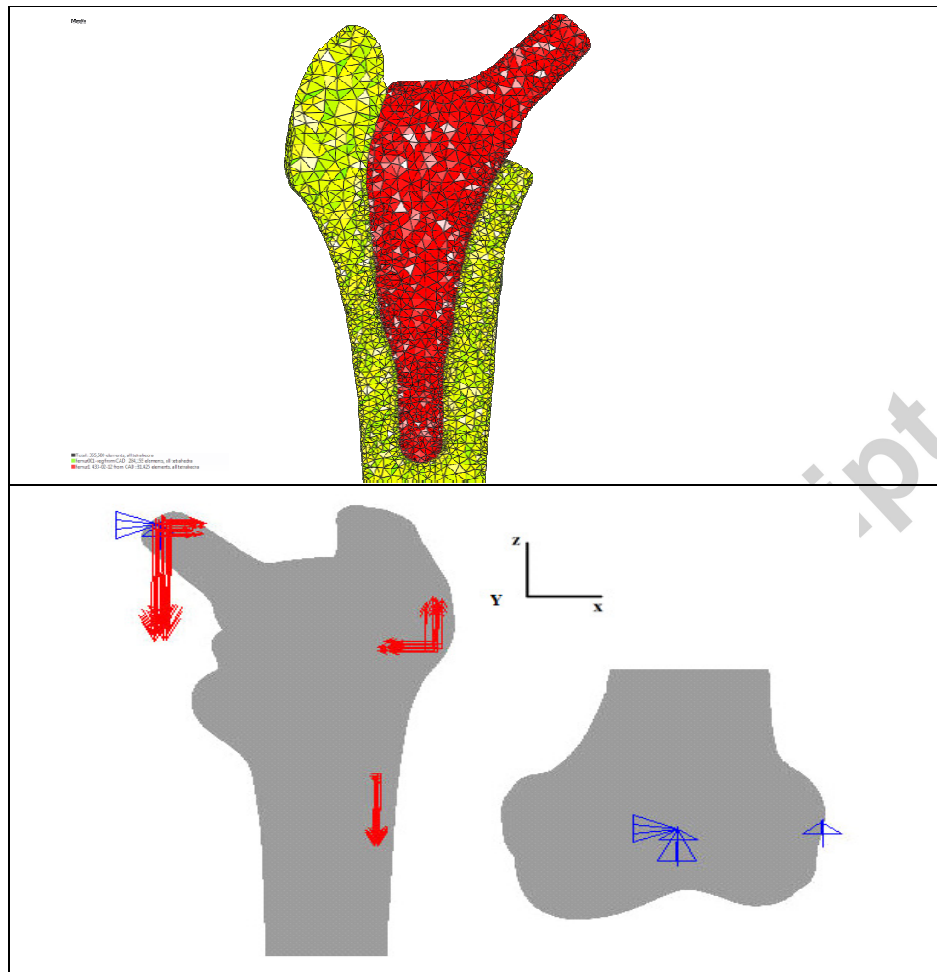
Figure 6: Relationship between standard canal flare index measured with respect to isthmus position and metaphyseal canal flare index. M: male; F: female.

Figure 7: Correlation chart between metaphyseal canal flare index, bone density and implant average micromotion (a) and sensitivity analysis results.

## List of Figures:

**Figure 1: Automated Anatomic Measurement and Implant Selection and Match Process.**





**Figure 2: Top plot shows a typical finite element mesh of an implanted femur model. Bottom plot shows distributed forces (hip contact, abductor, tensor fasciae latae and vastus lateralis) and constrained nodes (hip centre deflects along an axis towards the knee centre fixed in all directions and the distal lateral epicondyle constrained in y-direction to prevent rigid body motion (Speirs et al., 2007)).**

**Figure 3: Anterior (left) and posterior (right) view of a typical implant micromotion distribution in three selected patients: two male patients aged 47 (top) and 37 (middle) years and in one female patient aged 83 (bottom). Grey areas correspond to micromotions over 50  $\mu\text{m}$ .**

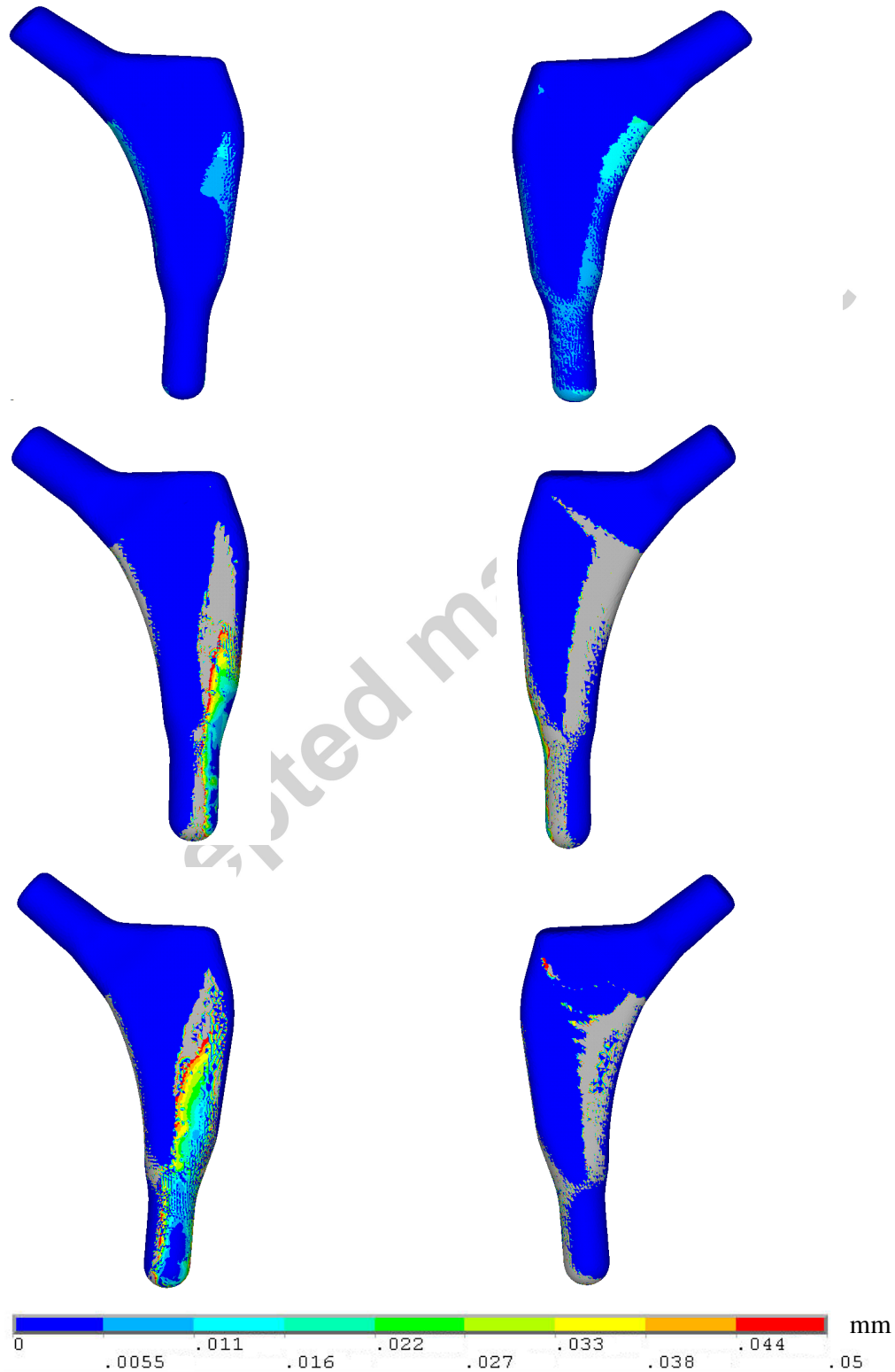
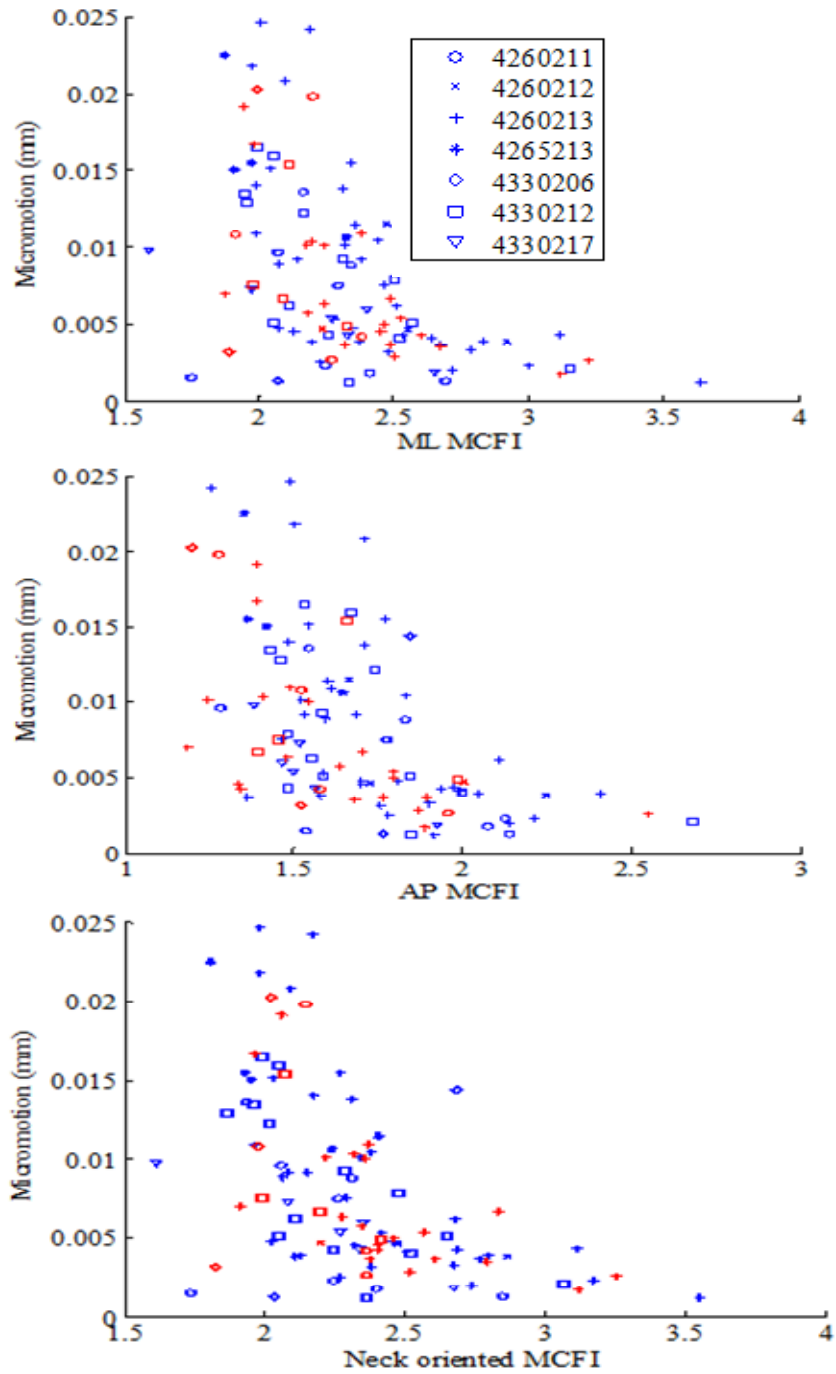


Figure 4: Changes of average micromotion against metaphyseal canal flare index. Females (red), Males (blue). Same legend as in Figure 5. Females (red), Males (blue). 426 and 433 refer to 126° and 133° CCD angle; 02 and 52 refer to standard (40.9mm) and high (45.9mm) neck offset; 11, 12, 13, 17 refer to stem distal size (mm).



**Figure 5: Changes of average micromotion against mean density in Gruen zones.**  
**Same legend as in Figure 3.**

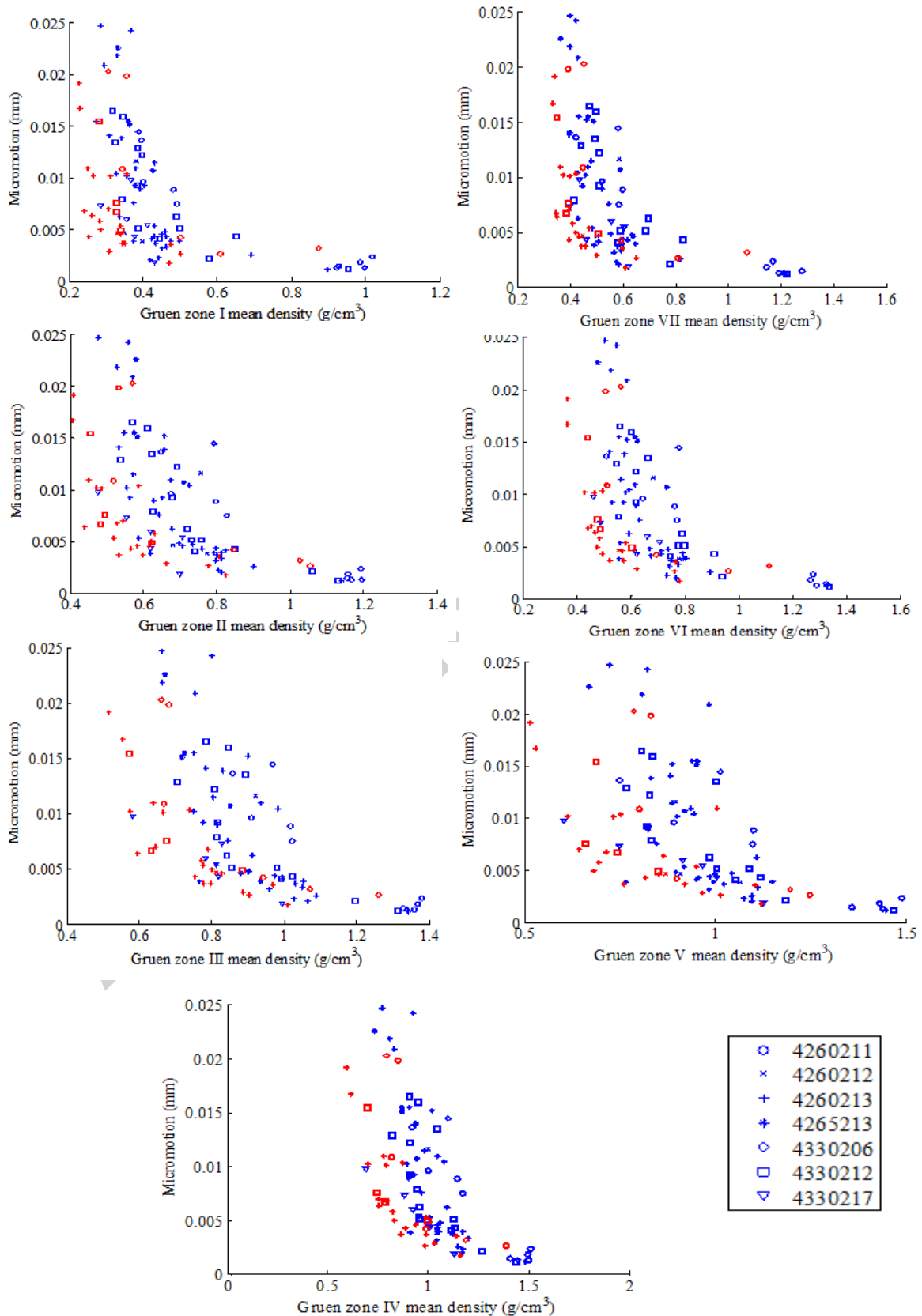


Figure 6: Relationship between standard canal flare index measured with respect to isthmus position and metaphyseal canal flare index. M: male; F: female.

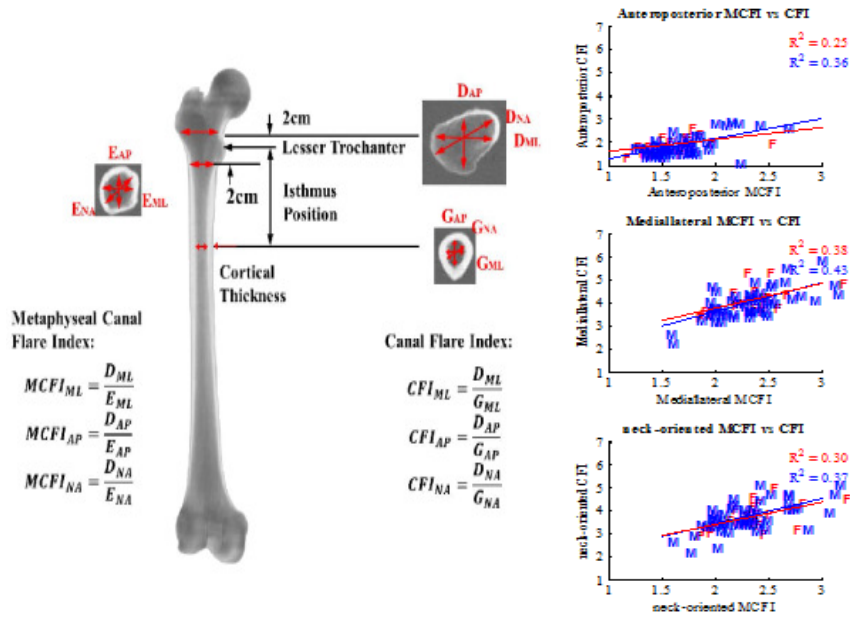
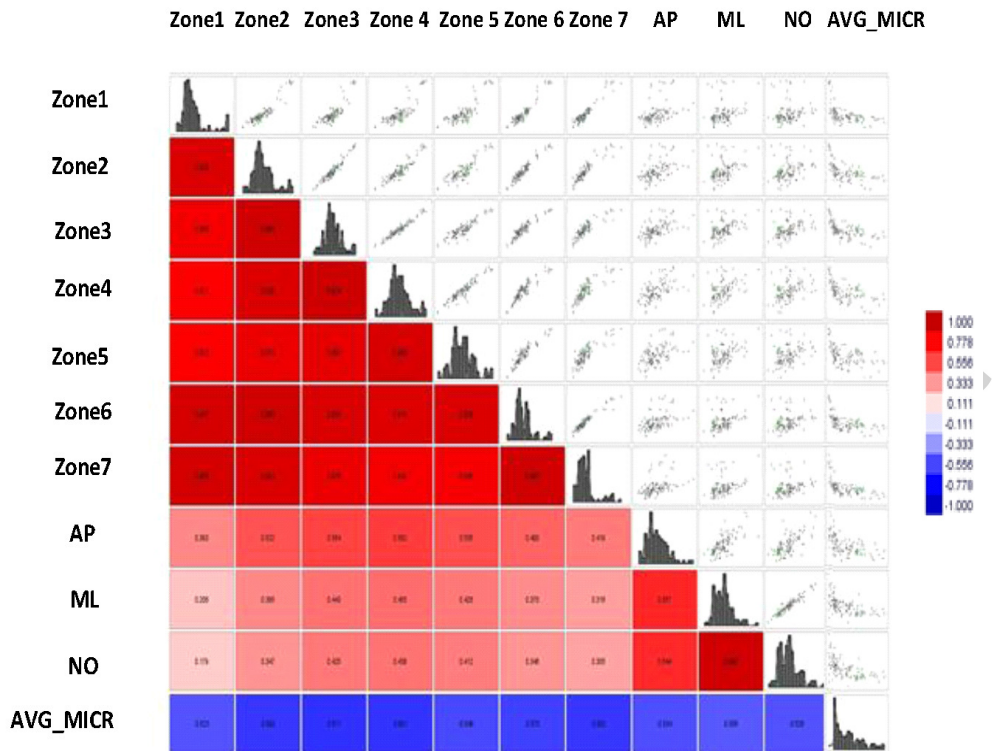


Figure 7: Correlation chart between metaphyseal canal flare index, bone density and implant average micromotion (a) and sensitivity analysis results.



(a)



(b)